water

MDPI

Article

Photocatalytic Removal of Dyes from Aqueous Medium by Fe, Mn and Fe-Mn Nanoparticles Synthesized Using *Cannabis sativa* Leaf Extract

Sadaf Naz [1], Rimsha Kalsoom [1], Faisal Ali [1], Nyla Amjed [1], Umer Younas [1,*], Muhammad Pervaiz [2,*], Mabkhoot Alsaiari [3,4], M. Faisal [3], Farid A. Harraz [3,5] and Rafael Luque [6,7,*]

1 Department of Chemistry, The University of Lahore, Lahore 53700, Pakistan
2 Department of Chemistry, Government College University Lahore, Lahore 54010, Pakistan
3 Promising Center for Sensors and Electronic Devices (PCSED), Advanced Materials and Nano Research Centre, Najran University, Najran 11001, Saudi Arabia
4 Empty Quarter Research Unit, Department of Chemistry, College of Science and Art in Sharurah, Najran University, Sharurah 61441, Saudi Arabia
5 Nanomaterials and Nanotechnology Department, Central Metallurgical Research and Development Institute (CMRDI), P.O. Box 87 Helwan, Cairo 11421, Egypt
6 Departamento de Quimica Organica, Universidad de Cordoba, Edificio Marie Curie (C-3), Ctra Nnal IV-A, Km 396, E14014 Cordoba, Spain
7 Peoples Friendship University of Russia (RUDN University), 6 Miklukho Maklaya Str., 117198 Moscow, Russia
* Correspondence: umer0608analyst@gmail.com (U.Y.); dr.mpbhatti@gcu.edu.pk or mpbhatti786@gmail.com (M.P.); q62alsor@uco.es (R.L.)

check for updates

Citation: Naz, S.; Kalsoom, R.; Ali, F.; Amjed, N.; Younas, U.; Pervaiz, M.; Alsaiari, M.; Faisal, M.; Harraz, F.A.; Luque, R. Photocatalytic Removal of Dyes from Aqueous Medium by Fe, Mn and Fe-Mn Nanoparticles Synthesized Using *Cannabis sativa* Leaf Extract. *Water* **2022**, *14*, 3535. https://doi.org/10.3390/w14213535

Academic Editor: Alexandre T. Paulino

Received: 1 October 2022
Accepted: 27 October 2022
Published: 3 November 2022

Publisher's Note: MDPI stays neutral with regard to jurisdictional claims in published maps and institutional affiliations.

Abstract: Current work describes green synthesis of Fe, Mn (monometallic) and Fe-Mn (bimetallic) nanoparticles using *Cannabis sativa* leaf extract as stabilizing and capping agent. In order to assess the formation of nanoparticles UV/Vis and FTIR analysis was carried out. In addition, Scanning electron microscopy and XRD studies confirmed synthesis as well as morphology of the nanoparticles. All the nanoparticles were found having particle size 20–80 nm and crystallite 3–20 nm. Photocatalytic activity of synthesized nanoparticles has been evaluated by carrying out degradation of two dyes methyl orange (MO) and Congo red (CR) in the presence of nanocatalysts. Degradation of both the dyes was carried out separately using Fe, Mn and Fe-Mn nanoparticles to compare the efficiency of monometallic with bimetallic nanoparticles. Iron and manganese monometallic particles have completely degraded MO in 18 min and 20 min and CR in 24 min and 18 min respectively. However, due to increased synergistic effect Fe-Mn BNPs completely degraded MO dye in just 12 min and CR in 14 min. In nutshell, this work is actually a step towards the synthesis of bimetallic nanoparticles using a plant extract with improved synergistic photocatalytic activities which impart various properties to the designed nanomaterial.

Keywords: bimetallic nanoparticles; photocatalytic activity; dye degradation; green synthesis; water treatment

1. Introduction

Industrial effluents having toxic pollutants are being released in the environment at massive level for the last several decades. These pollutants are causing severe damage to our environment and causing serious health issues [1,2]. Exposure of these pollutants may cause skin damage, vomiting, jaundice, tissue narcosis and quadriplegia like diseases in human beings. Among many other industries, dye based industries have been reported contributing about 10–15% of the total effluent discharged by different industries. The amount of different dyes released by these industries causes hindrance in development of aquatic species as it reflects or absorb sunlight radiation [3]. Degradation of dyes into less toxic substances cannot be done with the help of conventional dye removal methods like

flocculation, coagulation, membrane filtration and adsorption. Conversion of the dyes to non-toxic counterparts is difficult due their high stability and complex structures [4]. In order to achieve dye degradation in an easy way, researchers are using green synthesized metal nanoparticles (NPs) as catalyst. Green synthesis approach of synthesizing NPs involves no use of toxic solvents and chemicals to avoid environmental pollution and unwanted byproducts [5].

Nanomaterials have gained attention for their applications in drug delivery, photocatalytic bioremediation [6,7], drug delivery [8,9], imaging [10,11], gene delivery [12] and electronic applications [13,14]. Scientists initially focused synthesis of monometallic NPs and their applications and nowadays bimetallic/ trimetallic NPs synthesis is being focused due to their enhanced synergistic effects in various applications [15,16]. Osama Eljamal and his coworkers enhanced the yield of biogas employing iron-copper bimetallic nanoparticles (BmNPs) [17]. Nanoparticles of noble metals are among most demanded catalysts owing to their viable use in industrial sector. Bimetallic NPs have far more interesting and useful optical, magnetic catalytic and medical properties; this enhancement of properties is due to the synergistic effect of monometallic that combines to form Bimetallic [18,19]. Iron oxide among all the metals have unique chemical and physical properties [20].

Cannabis sativa belongs to cannabaceae family, distributed worldwide with great medicinal properties and commonly known as a factory of secondary metabolites including phenolics, lignins and alkaloids. Terpenes are important or vital class of compounds present in *C. sativa* and the characteristic odour of the crop belong to terpenes. *C. sativa* plants with height 1–5 m are available whole year, depending upon its genetic and environmental factors. Availability of the plant throughout the year is a great attraction for the scientists to explore its benefits. Keeping in view all the features associated with the plant, Fe, Mn and Fe-Mn NPs have been synthesized using its extract [18,19]. Authors have reported green synthesis of Au [21], Ag [22] and ZnO NPs using *Cannabis sativa* plant extract.

Keeping in view the importance of Fe NPs [23] and Mn NPs [24], authors planned current research work in continuation to our previous studies describing green synthesis of bimetallic NPs [25,26]. In this work, for the first time NPs of Fe, Mn and Fe-Mn (bimetallic) has been synthesized by green synthesis approach using *C. sativa* leaves extract as capping or stabilizing agent. In addition to complete characterization, the synthesized NPs were tested for their dye degradation potential. For the purpose, photocatalytic degradation of Methyl orange (MO) and Congo red (CR) has been carried out. Monometallic NPs (Fe and Mn) and bimetallic NPs (Fe-Mn) were compared in terms of their photocatalytic degradation potential to uncover the synergistic association of two metals in nanomaterials.

2. Materials and Methods

2.1. Chemicals and Reagents

The metal salts, solvents and all other chemicals used for this research were of analytical grade and thermally stable. Ferric chloride $FeCl_3$ (99.98%), Manganese chloride $MnCl_2$ (99.99%) were Purchased from Sigma Aldrich Germany. Methyl orange (99%) and Congo red dye (99%) acquired from Fischer Scientific UK.

2.2. Preparation of Plant Extract

Leaves of *Cannabis sativa* plant were obtained from different areas of Lahore, Punjab, Pakistan. These leaves were processed through preliminary steps of washing and drying under shade. In order to achieve constant weight of the sample, drying was carried out using hot oven at 60 °C for 3 h To prepare a laboratory sample leaves were then cut and ground to powder. Extract of *C. sativa* leaves was prepared in methanol and is stirred in orbital shaker for 3 h at 150 rpm. Drying of filtrate was done by rotary evaporator at −4 °C and stored prior further use [27].

2.3. Synthesis of Monometallic (Fe and Mn) Nanoparticles

Iron chloride and Manganese chloride salts were used for the synthesis of Monometallic Fe and Mn NPs. Both the metal salt (Fe and Mn) solutions were taken as precursor to metal nanoparticle synthesis. Solutions of both the salts (0.1 M, 10 mL) were prepared and 5 mL of *C. sativa* leaf extract was added to each salt solution. Sodium hydroxide solution (0.1 N) was added to maintain the pH at 8-9. Appearance of slight turbidity and color change indicated the synthesis of NPs. Both the solutions were separately centrifuged and dried at 70 °C for 3 h. The dried material thus obtained is stored for characterization [28,29].

2.4. Synthesis of Bimetallic (Fe-Mn) Nanoparticles

Bimetallic (Fe-Mn) nanoparticles were synthesized by using a salt solution prepared by mixing $FeCl_3$ and $MnCl_3$. The extract solution was diluted using methanol solvent to achieve 200 ppm concentration. Bimetallic nanoparticles were synthesized by mixing the salt solution (0.1 M, 25 mL) and *C. sativa* extract solution (200 ppm, 10 mL). Sodium hydroxide solution (0.1 N) was added to maintain the pH at 8–9. Change in solution color indicated the formation of BmNPs, which were then recovered by centrifugation and dried at 65 °C for 2 h [25,26].

2.5. Characterization of Nanoparticles

Synthesis of the NPs was confirmed by UV-visible spectrophotometric analysis performed using CECIL-7400ce UV-VIS-spectrophotometer, FTIR analysis by an IR prestige 21 Shimadzu, Kyoto, Japan. Crystallinity index was confirmed by using X-ray diffractometer (Bruker X-ray diffractometer, Coventry, UK), equipped with a scintillation counter using Cu Kα radiation (k = 1.5405 Å, nickel filter. SEM micrographs were obtained by Nova SEM recorded at 3 different resolutions.

2.6. Photocatalytic Degradation of Selected Dyes

Photocatalytic potential of Fe-Mn BmNPs was evaluated employing an already reported method. According to this method, methyl orange (0.076 mM) and Congo red (0.063 mM) solutions were prepared. In 10 mL solution of dye, 3mL solution of Fe NPs (100 ppm) was added followed by exposure to UV radiations (365 nm). Spectra of the resulting mixture were recorded using spectrophotometer. In the same way, photocatalytic potential of Mn and Fe-Mn NPs was evaluated against both the selected dyes [30,31].

3. Results and Discussion

Nanoparticles of Fe, Mn and Fe-Mn were synthesized via green route using *C. sativa* extract. In synthesis reaction, metal ions in salt solutions were allowed to react with phytochemical present in the extract. Metal ions from their respective salts were used as precursor to nanoparticles. Phytochemicals contributed in reducing and stabilizing the metal atoms for the formation of nanoparticles. Synthesized nanoparticles were characterized employing different analytical techniques including UV-visible, FTIR, SEM and XRD. Catalytic potential of monometallic (Fe and Mn) and bimetallic (Fe-Mn) NPs was compared in term of their dye degradation potential.

3.1. UV-Vis Characterization of Nanoparticles

The analysis of the synthesized NPs was done using UV-visible spectrophotometer (Figure 1) and absorbance was observed ultraviolet region [26]. Literature studies show that the absorbance of Fe-NPs has been reported in the range of 280–350 nm. In current work the spectra exhibited maximum absorbance peak at 300 nm that confirmed the formation of Fe-NPs by using *C. sativa* leaves extract [32,33]. UV-visible spectroscopic analysis of Mn-NPs was also performed and peak appeared (Figure 1) in the spectrum at 370 nm. According to the literature, absorbance range for Mn-NPs is 360–417 nm which supports the results of current study and formation of Mn-NPs [34]. Preliminary analysis of the Fe-Mn BmNPs carried out using UV-vis spectrophotometer confirmed the formation of

NPs synthesized using *C. sativa* leaves extract. Representative peaks of Fe and Mn NPs can be seen in the spectrum of Fe-Mn BmNPs which confirmed the formation of BmNPs.

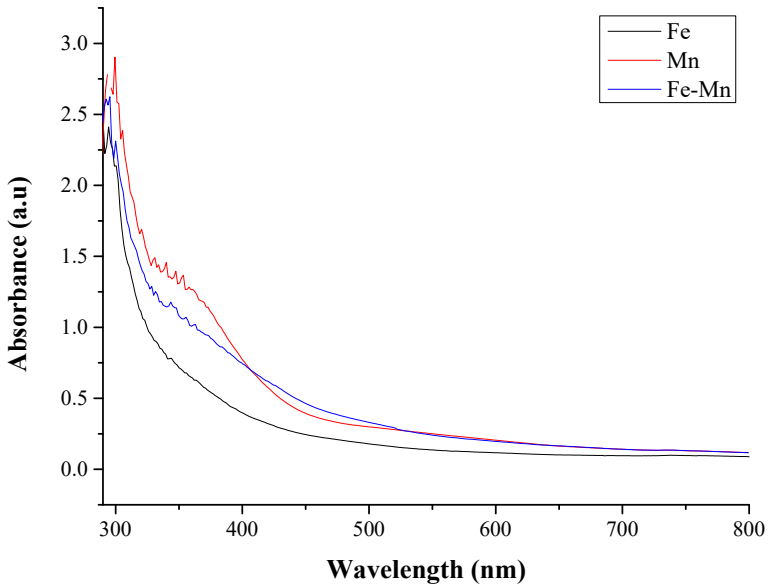

Figure 1. UV-visible spectra of Fe, Mn and Fe-Mn NPs.

3.2. FTIR Analysis of Nanoparticles

Analysis of synthesized NPs was carried out employing FTIR spectroscopic technique and presented in Figure 2. In Figure 2a, a dip around 3266.57 cm^{-1} appeared due to the presence of C-H group stretching in tetrahydrocannabinol and hydroxyl (O-H) and oxygen group stretching of cannabidiol obtained from *C. sativa* leaves extract. The stretching vibrations at 1613.99 cm^{-1} may probably be assigned to the N-H stretching of amines and C=O stretching of amide bonds associated with protein molecules. The dip around 1383.81 cm^{-1} was due to C=C stretching and peak at 1044.09 cm^{-1} indicated the presence of C-O-C stretching [26]. In Figure 2b, spectra of Mn NPs has been presented and a dip around 3312.82 cm^{-1} was recorded due to stretching vibrations of C-H and O-H group present in sample [26]. Another dip around 1557.20 cm^{-1} appeared due to the vibrations of N-H [35] and peak at 1662.63 cm^{-1} may be due to C=O group stretching [26]. The peaks at 1393.46 cm^{-1} and 1048.06 cm^{-1} indicated the presence of C=C and C-O-C stretching vibrations respectively [25]. It is clear from the spectra that specific functional groups detected in different compounds extracted from leaves have been found involved in stabilizing Fe and Mn NPs.

Bimetallic nanoparticles (Fe-Mn) were also analyzed using FTIR technique and dip around 3266 cm^{-1} was due to the presence of C-H and O-H group in the sample. Another dip around 1608 cm^{-1} was due to the presence of stretching vibrations of N-H group in amines and C=O stretching of amide bond due to protein molecules. The peaks at 1348 cm^{-1} and 1046 cm^{-1} indicates the presence of C=C and C-O-C stretching respectively. Peaks appeared around 1600 cm^{-1} in spectra of Fe and Fe-Mn confirmed the presence of Fe in BmNPs. In addition, peaks observed at 901 cm^{-1} and 730 cm^{-1} may be attributed to Mn derived NPs [34]. FTIR spectra recorded for Fe-Mn BmNPs confirmed the presence of Fe, Mn and phytochemicals extracted from *C. sativa* leaves.

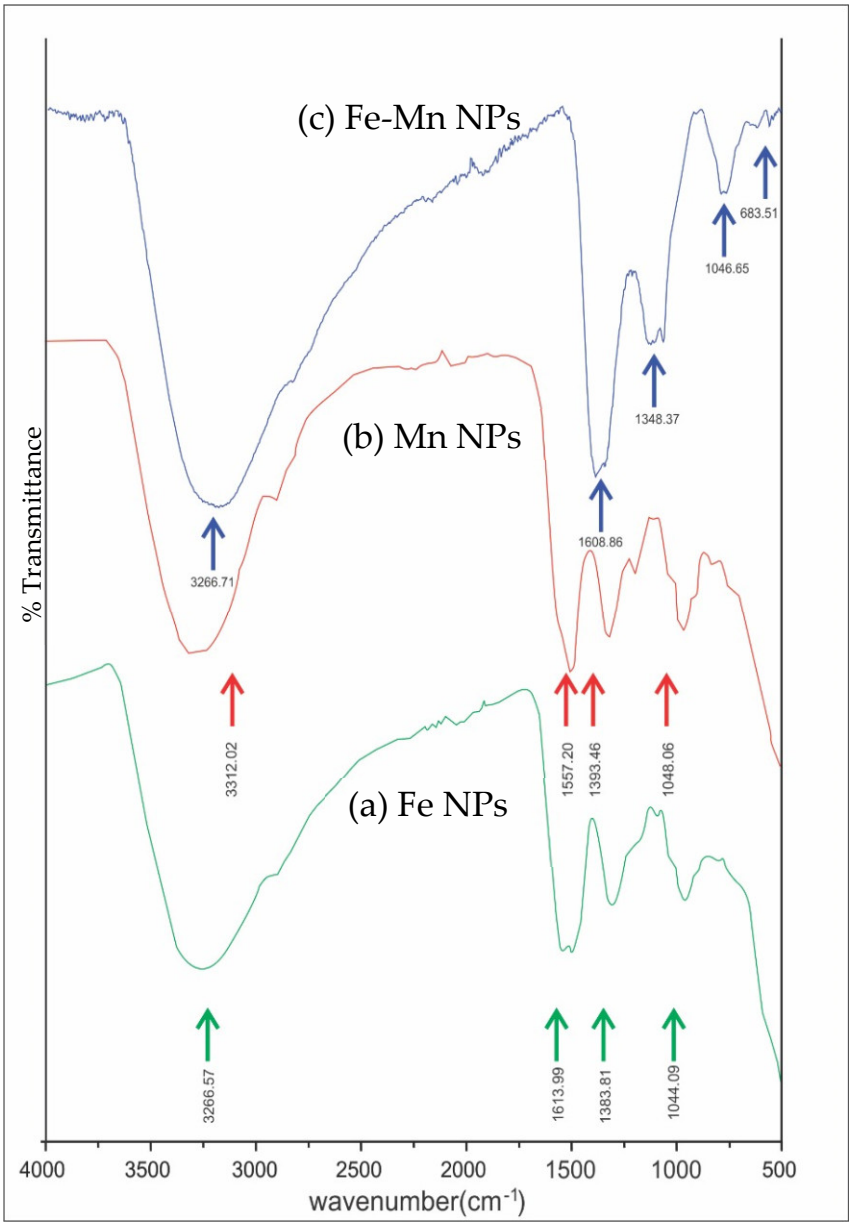

Figure 2. FTIR spectra of (**a**) Fe NPs, (**b**) Mn NPs (**c**) Fe-Mn NPs.

3.3. XRD Studies

Nanoparticles (Fe, Mn and Fe-Mn) synthesized using *C. sativa* extract were analyzed using X-ray diffractometer and spectra have been presented in Figure 3. According to the Figure 3, XRD spectra recorded for Fe NPs (Table 1), miller indices values at 2θ i.e., 31.79, 42.45, 44.66, 47.39, 49.41, 65.99 are (100), (100), (101), (104), (102), (104) respectively. The presence of characteristic peaks at 32°, 42°, and 57° corresponding to Hematite (α-Fe_2O_3), whereas the peak at 44° correspond to zerovalent iron (α-Fe) phase (JCPDS No: 50-1275) [36]. The presence of some other peaks may be due to impurities of bio substances. The sharp and intense peaks confirmed the presence of Fe NPs and their hexagonal (primitive) nature. The average crystalline size was 10.70 nm (Table 1) as calculated by Debye-Scherrer equation.

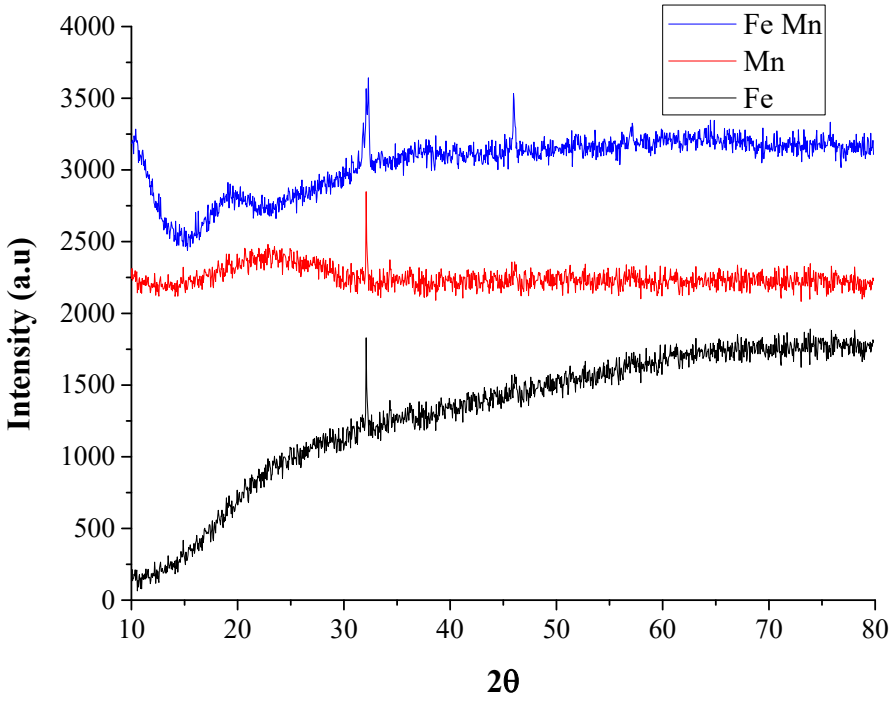

Figure 3. XRD spectra Fe, Mn and Fe-Mn NPs.

Table 1. XRD Diffraction Pattern of Fe NPs.

2 Theta (deg)	M.I (hkl)	d Pacing	FWHM	Crystallite Size
31.79	100	2.8126	0.10528	11.94061
42.45	100	2.1018	0.04379	24.70497
44.66	101	2.0270	0.9992	1.052824
47.39	104	1.9165	0.57504	1.741224
49.41	102	1.8429	0.05196	18.5197
65.9	104	1.4162	0.09656	6.254256

The morphology and structure of Mn NPs was also identified using XRD diffraction pattern (Figure 3). The peaks recorded (Table 2) at 22°, 28° 32°, 36°, 45°, 56°, 63°, 65° correspond to (111), (210), (211), (220), (320), (410), (331), (421) miller indices for Manganese NPs (JCPD No: 21-0547) [37]. Crystal phase identification of Mn NPs was achieved by using XRD with CuKa1 λ = 1.5406Å. Sharp peaks indicated the cubic nature of Mn NPs. The average crystallite size found to be 18.17 nm (Table 2) was estimated by Debye-Scherrer formula.

Table 2. XRD Diffraction Pattern of Mn NPs.

2 Theta (deg)	M.I (hkl)	d Spacing	FWHM	Crystallite Size
22.86	111	4.0300	0.10675	12.84302
28.68	210	3.1300	0.02312	56.22286
32.07	211	2.8440	3.64897	0.345882
36.13	220	2.4720	0.59902	1.989576
45.98	320	1.9350	0.14555	7.212654
54.02	410	1.6960	0.02891	30.05543
57.16	331	1.6100	0.022	36.45642
60.50	1.5290	421	2.77674	0.26228

Structural integrity of BmNPs was evaluated employing XRD diffractometer. In this analysis, 2 θ scale was plotted against intensity (Figure 3) illustrating that miller indices for diffraction peaks at 32.66, 44.32, 51.90, 65, 54, 76.69 are (210) (221) (320) (410) (332)

430) respectively (Table 3). The peaks appearing at 32° relates to hematite (α-$Fe_2O_{3)}$ while another peak appearing at 45° depicting the presence of zerovalent iron phase [36] and the peaks at 51°, 57°, 69° [37] and 75° [38] correspond to the manganese NPs. Theta values indicating that the synthesized material is highly crystalline and cubic in nature. No extra peak appeared in the XRD spectrum of BmNPs ensuring about the purity of product. The average size of BmNPs was estimated by Debye-Scherrer equation was about 0.63 nm (Table 3). XRD patterns appeared in Fe and Mn spectra, synergistically observed in XRD pattern recorded for bimetallic Fe-Mn NPs. However, difference in d spacing values of bimetallic particles is less as compared to their monometallic products, validating the increase in crystallinity of nanocomposites.

Table 3. XRD Diffraction Pattern of Fe-Mn BNPs.

2 Theta (deg)	M.I (hkl)	d Spacing	FWHM	Crystallite Size D
32.66	2 1 0	0.2166265	8.97065	0.1582146
44.32	2 2 1	0.2905815	17.70622	0.0773574
51.90	3 2 0	0.3371019	0.42078	3.1604
59.32	4 1 0	0.381237	15.15031	0.0848259
65.45	3 3 2	0.4164671	4.57589	0.2718989
76.69	4 3 0	0.4779015	23.79657	0.0487435

3.4. SEM Analysis

In order to assess the morphology of the NPs synthesized using *C. sativa* leaves extract, SEM images were obtained using NOVA Nano SEM 450 at different magnifications as shown in Figure 4a,b (1 µm, 200 nm). It has been observed that Fe NPs are heterogeneous mixture and recorded micrographs display a mixed morphology of triangular and rectangular NPs. The variations in particle sizes occurred due to the clumping of NPs. By increasing the magnification (200 nm), various morphologies of NPs observed because of the interactions of extract biomolecules with NPs [25,26].

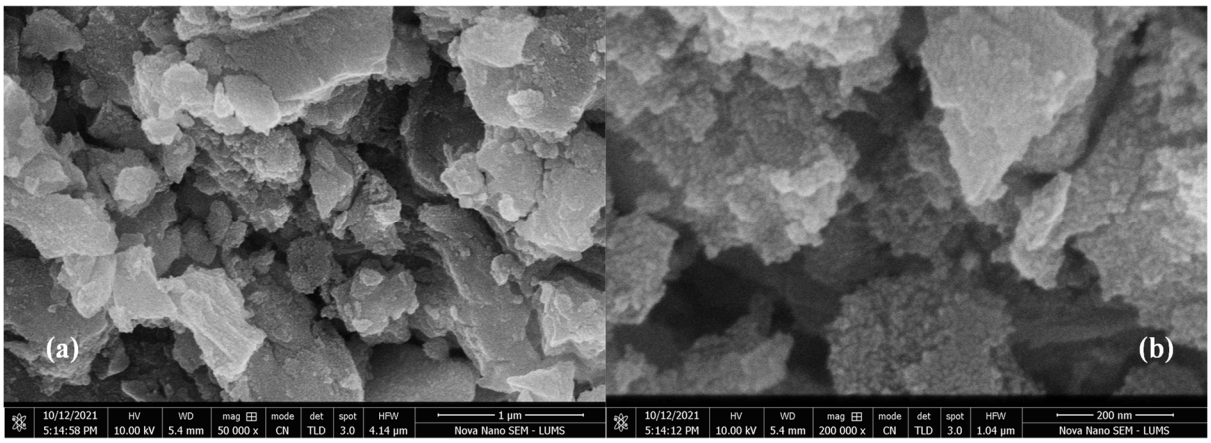

Figure 4. SEM micrographs of Fe NPs at 1 µm (**a**), 200 nm (**b**).

Nanoparticles of manganese synthesized using *C. sativa* leaves extract were examined for their morphology and SEM micrographs were recorded at different magnification Figure 5a,b (1 µm, 200 nm). SEM images revealed that the NPs were having heterogeneous morphology due to clumping of NPs and are not completely spherical in shape. Nanoparticles are self-assembled together to form cluster formation [26].

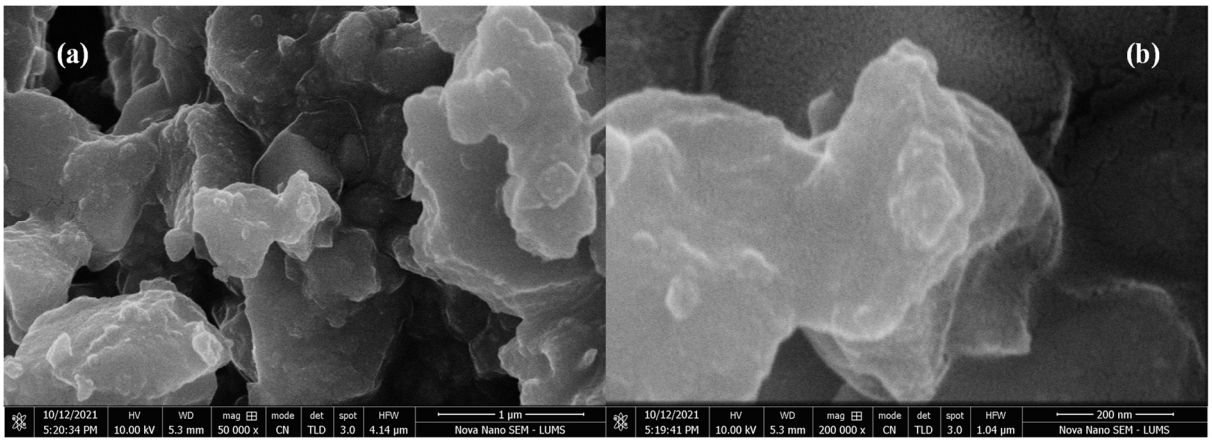

Figure 5. SEM micrographs of Mn NPs at 1 µm (**a**), 200 nm (**b**).

SEM micrographs of bimetallic Fe-Mn particles are displayed in Figure 6a,b (1 µm, 200 nm). It is observed from this figure that BmNPs exhibit heterogeneous surfaces. The overall view of NPs can be seen at two different magnifications. The randomly arranged particles in SEM micrographs depicted their agglomeration or cluster formation might be owing to its interaction with bio moieties. Moreover, at high resolution particles are representing square and oval-shaped morphology. Definite boundaries of particles are clearly visible in images and particles have compact surface without any visible pores [39].

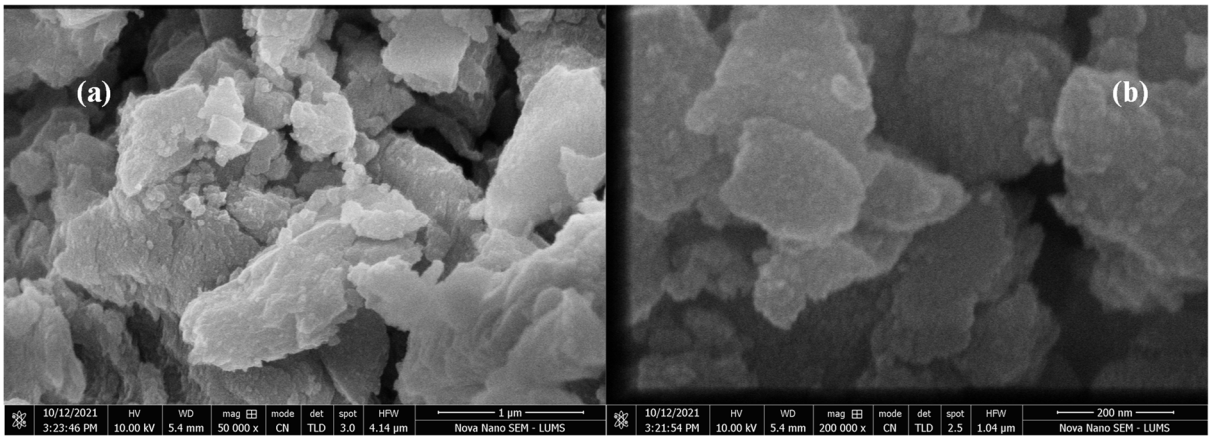

Figure 6. SEM micrographs of Fe/Mn NPs at 1 µm (**a**), 200 nm (**b**).

3.5. Photocatalytic Activity

Many researchers have reported synthesis and catalytic activity of metal NPs for the degradation of dyes. Huge amount of dyes is disposed into ground water resources that are seriously damaging the environment as these dyes can cause serious hazards to aquatic life and several health issues to human. Dyes are being removed from aqueous medium by the process of photocatalytic degradation using metal NPs [40,41]. Metal NPs synthesized in current work using *C. sativa* extract, were tested for photocatalytic activity against two selected dyes i.e., degradation of methyl orange and Congo red was achieved.

Degradation of MO

Methyl orange is an azo dye has been widely used in many industries. Degradation of MO was carried out using Fe, Mn and Fe-Mn NPs. In the absence of a catalyst, reduction of MO was not observed. This may happened due to the presence of high energy barrier to initiate the degradation reaction [41]. Degradation of MO dye was done in the presence of

Fe NPs and spectra were recorded after regular time intervals using UV-visible spectrophotometer (Figure 7). Photocatalytic degradation (up to 85%) of MO dye was successfully completed in within just 18 min. Fe NPs synthesized in current work exhibited much better efficiency as compare to the efficiency of previously reported Fe NPs [42].

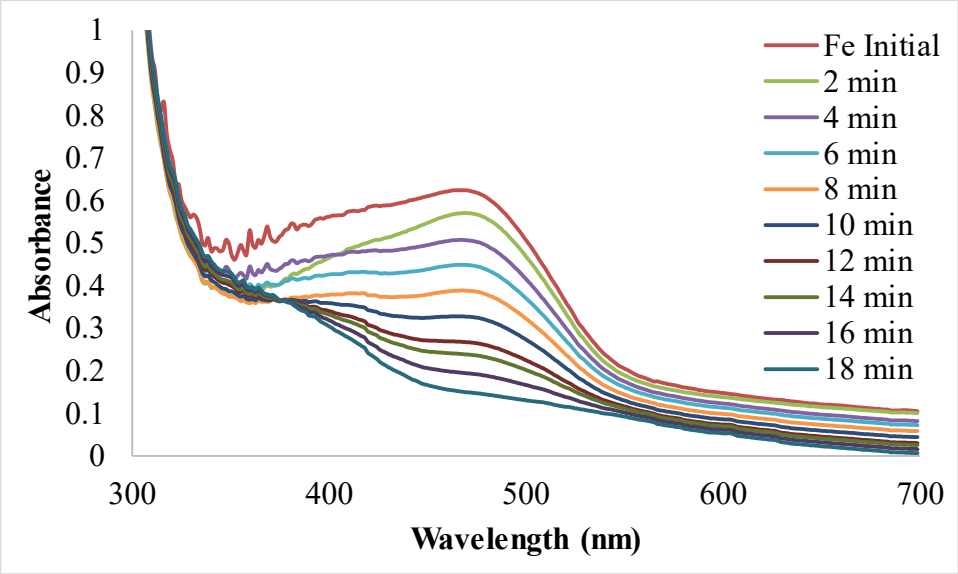

Figure 7. UV-visible spectra for photocatalytic degradation of MO using Fe NPs.

Photocatalytic degradation potential of Mn NPs was also tested against MO dye. Degradation of MO dye was carried out in the presence of nanocatalyst i.e., Mn NPs. Spectra of the dye were recorded after regular time intervals in the presence of the catalyst (Figure 8). Results revealed that degradation of MO dye was achieved up to 80% within 20 min. For the degradation of dye, Fe NPs were found better as compare to Mn NPs.

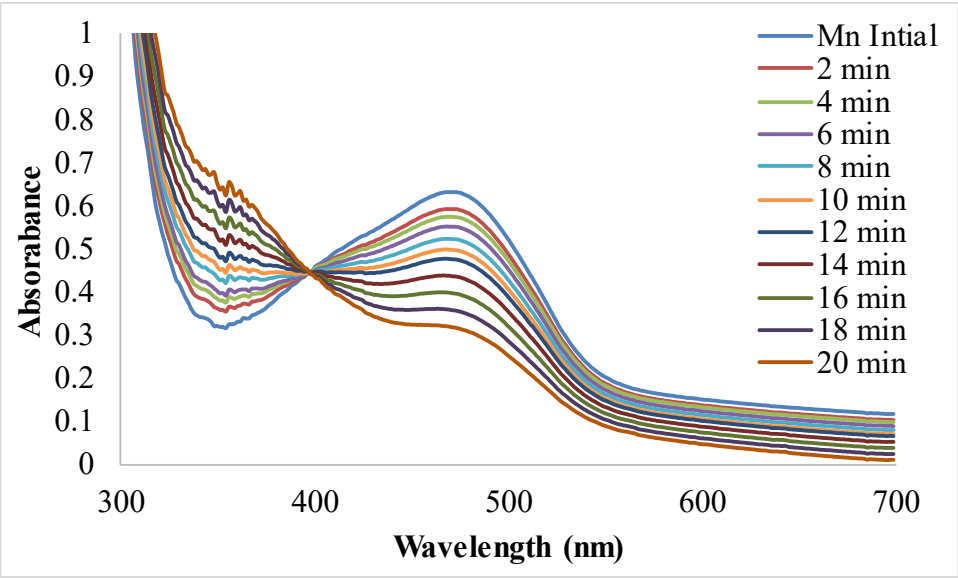

Figure 8. UV-visible spectra for photocatalytic degradation of MO using Mn NPs.

Green synthesized Fe-Mn BmNPs were evaluated for their photocatalytic degradation of MO dye. For this purpose, same optimized conditions were used as that for Fe and Mn NPs. Bimetallic nanoparticles exhibited excellent efficiency for the degradation of MO. The

results presented in Figure 9 revealed that the degradation by BmNPs was found to be more effective then monometallic NPs (Fe and Mn), In case of BmNPs degradation was achieved just in 12 min with 90 % degradation efficacy and it is an evident for the association of metals in BmNPs as well as synergistic effects of the BmNPs [43].

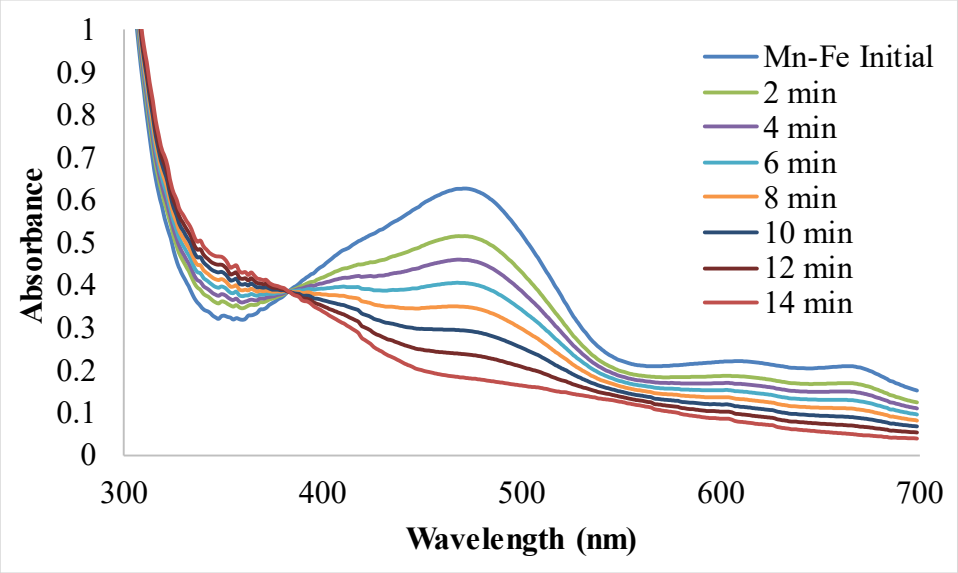

Figure 9. UV-visible spectra for photocatalytic degradation of MO using Fe-Mn NPs.

3.6. Degradation of CR

Degradation of CR dye was also achieved in the presence of Fe, Mn and Fe-Mn NPs synthesized using *C. sativa* leaves extract. Photocatalytic activity of Fe NPs was recorded after regular time intervals, specific conditions and under the effect of UV radiations. The spectra recorded for CR dye has been presented in Figure 10 that confirmed the degradation up to 90 % in 24 min. In a previously reported work, degradation of CR dye was achieved in almost 60 min which indicate that Fe NPs synthesized in current work are efficient in nature [44].

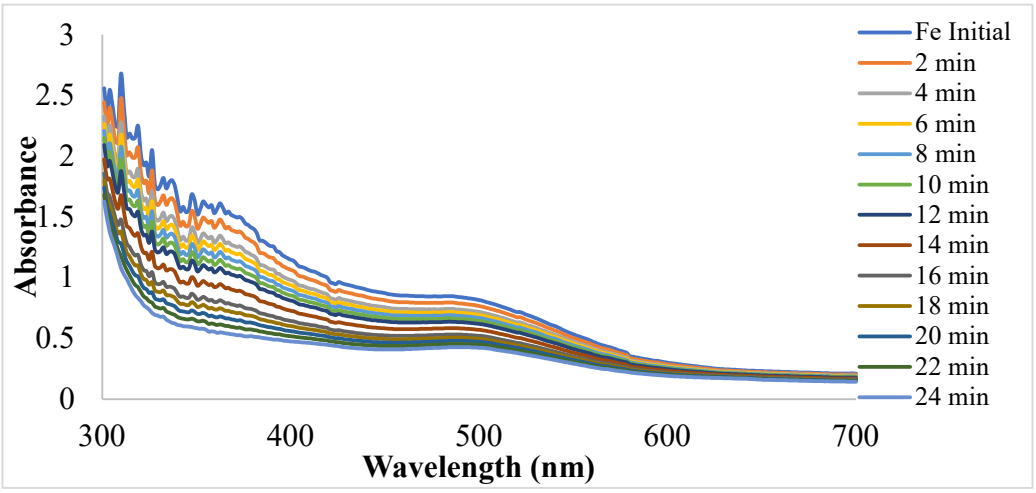

Figure 10. UV-visible spectra for photocatalytic degradation of CR using Fe NPs.

Degradation of CR dye was carried out using Mn NPs to evaluate the photocatalytic potential of synthesized monometallic NPs. All the conditions throughout the degradation studies were kept constant. The results of CR degradation were assessed by spectra

presented in Figure 11 that shows decrease in intensity of CR dye solution after regular time intervals in the presence of Mn NPs. Degradation potential of the Mn NPs was effective then Fe NPs, as degradation was achieved in just 18 min. Efficiency of Mn NPs for the degradation of CR was found better than previously reported results in which degradation up to 75% was completed in 80 min using Mn NPs [45].

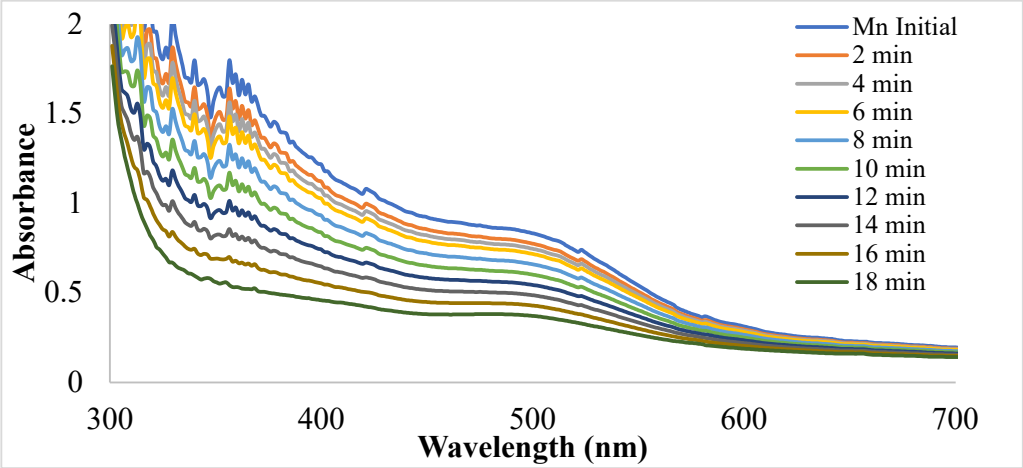

Figure 11. UV-visible spectra for photocatalytic degradation of CR using Mn NPs.

To examine the photocatalytic potential of the synthesized Fe-Mn BmNPs in comparison with their monometallic counterparts, degradation of CR dye was carried out. The results have been presented as spectra of CR in Figure 12 which confirms reduction was more effective than monometallic NPs of Fe and Mn, occurred within just 12 min. Experimental work is showing that Fe-Mn BNPs are more effective for degradation of CR dye as compared to monometallic NPs of Fe and Mn. In case of Fe NPs and Mn NPs, intensity of the dye solution was completely decreased in 18 and 20 min but in case of Fe-Mn BmNPs, degradation is completely occurred within just 12 min.

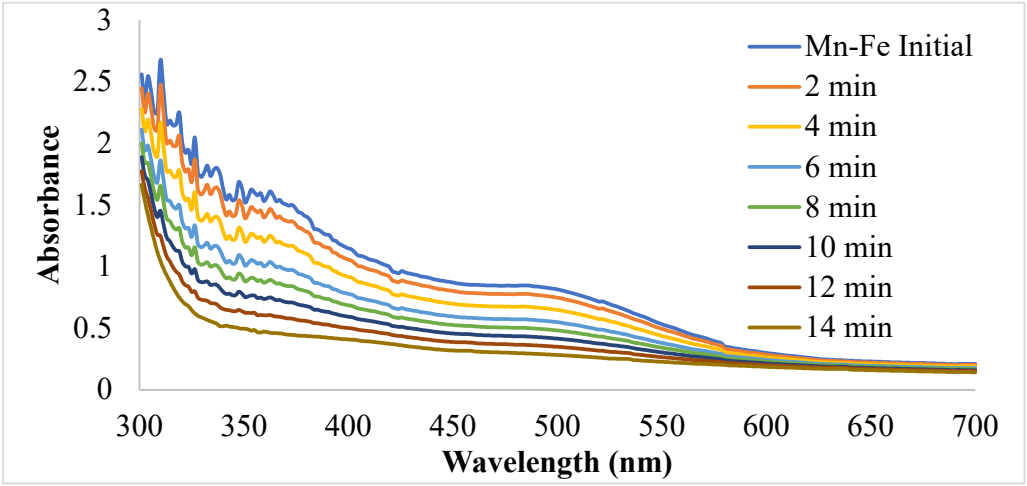

Figure 12. UV-visible spectra for photocatalytic degradation of CR using Fe-Mn NPs.

4. Conclusions

Current work was designed to synthesize monometallic and BmNPs involving similar metal atoms and extract obtained from same botanical material. Nanoparticles such as Fe, Mn and Fe-Mn have been synthesized using *C. sativa* leave extract. The plant extract efficiently acted as reducing and stabilizing agents for the metal NPs. Preliminary UV and FTIR spectroscopic analysis confirmed the synthesis of NPs. Other characterization

techniques such as XRD and SEM investigations provided crystallinity index and nano dimensions of the synthesized NPs. Authors concluded that phytochemicals present in plant extracts possess potential to synthesize both monometallic and BmNPs. Photocatalytic potential of the synthesized NPs was evaluated using a methyl orange and Congo red dyes. Results revealed that the synthesized bimetallic particles can be effectively employed for the degradation of the dye present in aqueous solution even more than monometallic NPs. Furthermore, these NPs can be exploited for the degradation of dyes that can be a good commodity for the treatment of water from textile industry. Moreover, current study will encourage green synthesis of bimetallic NPs that is ecofriendly, have gained much importance in nanotechnology now a day.

Author Contributions: Conceptualization, F.A.; methodology, U.Y.; software, F.A.H.; validation, M.A.; formal analysis, M.F.; investigation, R.K.; resources, N.A.; original draft preparation and editing, U.Y.; supervision, S.N.; project administration, M.P.; funding acquisition, R.L. All authors have read and agreed to the published version of the manuscript.

Funding: This research was funded by the grant (NU/IFC/INT/01/003) under the institutional funding committee at Najran University, Kingdom of Saudi Arabia.

Data Availability Statement: Not applicable.

Acknowledgments: The authors would like to acknowledge the support of the deputyship for research and innovation-Ministry of Education, Kingdom of Saudi Arabia for this research through grant (NU/IFC/INT/01/003) under the institutional funding committee at Najran University, Kingdom of Saudi Arabia.

Conflicts of Interest: The authors declare no conflict of interest.

References

1. Rajan, A.J.; Anand, K.T.; Narayanan, K.V.; Bapu, B.R.R. A Study on Environmental Sustainability in Textile Processing Industries of South India. *Indian J. Sci. Technol.* **2016**, *9*, 1–4. [CrossRef]
2. Zhu, S.; Khan, M.A.; Kameda, T.; Xu, H.; Wang, F.; Xia, M.; Yoshioka, T. New insights into the capture performance and mechanism of hazardous metals Cr^{3+} and Cd^{2+} onto an effective layered double hydroxide based material. *J. Hazard. Mater.* **2022**, *426*, 128062. [CrossRef]
3. Sannino, D. Mathematical modelling of photocatalytic degradation of methylene blue under visible light irradiation. *J. Environ. Chem. Eng.* **2013**, *1*, 56–60. [CrossRef]
4. Ahmed, M.J. Plants: Emerging as Green Source toward Biosynthesis of Metallic Nanoparticles and its Applications. *J. Bioprocess. Chem. Eng.* **2014**, *2*, 1–7.
5. Ebrahiminezhad, A.; Zare-Hoseinabadi, A.; Berenjian, A.; Ghasemi, Y. Green synthesis and characterization of zero-valent iron nanoparticles using stinging nettle (*Urtica dioica*) leaf extract. *Green Process. Synth.* **2017**, *6*, 469–475. [CrossRef]
6. Vasantharaj, S. Biosynthesis of iron oxide nanoparticles using leaf extract of *Ruellia tuberosa*: Antimicrobial properties and their applications in photocatalytic degradation. *J. Photochem. Photobiol. B Biol.* **2019**, *192*, 74–82. [CrossRef]
7. Ebrahiminezhad, A.; Taghizadeh, S.; Ghasemi, Y.; Berenjian, A. Green synthesized nanoclusters of ultra-small zero valent iron nanoparticles as a novel dye removing material. *Sci. Total Environ.* **2017**, *621*, 1527–1532. [CrossRef]
8. Khalil, A.T. Biosynthesis of iron oxide (Fe_2O_3) nanoparticles via aqueous extracts of *Sageretia thea* (Osbeck.) and their pharmacognostic properties. *Green Chem. Lett. Rev.* **2017**, *10*, 186–201. [CrossRef]
9. Niraimathee, V.; Subha, V.; Ravindran, R.E.; Renganathan, S. Green synthesis of iron oxide nanoparticles from *Mimosa* pudica root extract. *Int. J. Environ. Sustain. Dev.* **2016**, *15*, 227–240. [CrossRef]
10. Sandiford, L.; Phinikaridou, A.; Protti, A.; Meszaros, L.K.; Cui, X.; Yan, Y.; Frodsham, G.; Williamson, P.A.; Gaddum, N.; Botnar, R.M.; et al. Bisphosphonate-Anchored PEGylation and Radiolabeling of Superparamagnetic Iron Oxide: Long-Circulating Nanoparticles for In Vivo Multimodal (T1 MRI-SPECT) Imaging. *ACS Nano* **2013**, *7*, 500–512. [CrossRef]
11. Cheong, S.; Ferguson, P.; Feindel, K.W.; Hermans, I.F.; Callaghan, P.T.; Meyer, C.; Slocombe, A.; Su, C.; Cheng, F.; Yeh, C.; et al. Simple Synthesis and Functionalization of Iron Nanoparticles for Magnetic Resonance Imaging. *Angew. Chem.* **2011**, *123*, 4292–4295. [CrossRef]
12. Kievit, F.M. PEI–PEG–chitosan-copolymer-coated iron oxide nanoparticles for safe gene delivery: Synthesis, complexation, and transfection. *Adv. Funct. Mater.* **2009**, *19*, 2244–2251. [CrossRef]
13. Mallikarjuna, N. Novel high dielectric constant nanocomposites of polyaniline dispersed with γ-Fe_2O_3 nanoparticles. *J. Appl. Polym. Sci.* **2005**, *97*, 1868–1874. [CrossRef]
14. Zhu, S.; Xia, M.; Chu, Y.; Khan, M.A.; Lei, W.; Wang, F.; Muhmood, T.; Wang, A. Adsorption and Desorption of Pb(II) on l-Lysine Modified Montmorillonite and the Simulation of Interlayer Structure. *Appl. Clay Sci.* **2019**, *169*, 40–47. [CrossRef]

15. Aravind, M.; Ahmad, A.; Ahmad, I.; Amalanathan, M.; Naseem, K.; Mary, S.M.M.; Parvathiraja, C.; Hussain, S.; Algarni, T.S.; Pervaiz, M.; et al. Critical green routing synthesis of silver NPs using jasmine flower extract for biological activities and photocatalytical degradation of methylene blue. *J. Environ. Chem. Eng.* **2021**, *9*, 104877. [CrossRef]
16. Sharma, G.; Kumar, A.; Sharma, S.; Naushad, M.; Dwivedi, R.P.; Alothman, Z.A.; Mola, G.T. Novel development of nanoparticles to bimetallic nanoparticles and their composites: A review. *J. King Saud Univ. Sci.* **2019**, *31*, 257–269. [CrossRef]
17. Amen, T.W. Methane yield enhancement by the addition of new novel of iron and copper-iron bimetallic nanoparticles. *Chem. Eng. Process.-Process Intensif.* **2018**, *130*, 253–261. [CrossRef]
18. Abbasi, B.H. Biogenic synthesis of Au, Ag and Au–Ag alloy nanoparticles using Cannabis sativa leaf extract. *IET Nanobiotech.* **2018**, *12*, 277–284. [CrossRef]
19. Berta, L.; Coman, N.-A.; Rusu, A.; Tanase, C. A Review on Plant-Mediated Synthesis of Bimetallic Nanoparticles, Characterisation and Their Biological Applications. *Materials* **2021**, *14*, 7677. [CrossRef]
20. Willard, M.; Kurihara, L.; Carpenter, E.; Calvin, S.; Harris, V. Chemically prepared magnetic nanoparticles. *Int. Mater. Rev.* **2004**, *49*, 125–170. [CrossRef]
21. Chang, Y.; Zheng, C.; Chinnathambi, A.; Alahmadi, T.A.; Alharbi, S.A. Cytotoxicity, anti-acute leukemia, and antioxidant properties of gold nanoparticles green-synthesized using *Cannabis sativa* L. leaf aqueous extract. *Arab. J. Chem.* **2021**, *14*, 103060. [CrossRef]
22. Csakvari, A.C. Green synthesis, characterization, and antibacterial properties of silver nanoparticles obtained by using diverse varieties of *Cannabis sativa* leaf extracts. *Molecules* **2021**, *26*, 4041. [CrossRef]
23. Saif, S.; Tahir, A.; Chen, Y. Green synthesis of iron nanoparticles and their environmental applications and implications. *Nanomaterials* **2016**, *6*, 209. [CrossRef]
24. Hoseinpour, V.; Ghaemi, N. Green synthesis of manganese nanoparticles: Applications and future perspective—A review. *J. Photochem. Photobiol. B Biol.* **2018**, *189*, 234–243. [CrossRef]
25. Younas, U. Radical scavenging and catalytic activity of Fe-Cu bimetallic nanoparticles synthesized from *Ixora* finlaysoniana extract. *Coatings* **2021**, *11*, 813. [CrossRef]
26. Younas, U.; Gulzar, A.; Ali, F.; Pervaiz, M.; Ali, Z.; Khan, S.; Saeed, Z.; Ahmed, M.; Alothman, A.A. Antioxidant and Organic Dye Removal Potential of Cu-Ni Bimetallic Nanoparticles Synthesized Using *Gazania rigens* Extract. *Water* **2021**, *13*, 2653. [CrossRef]
27. Sharma, Y.; Kawatra, A.; Sharma, V.; Dhull, D.; Kaushik, S.; Yadav, J.P.; Kaushik, S. In-vitro and in-silico evaluation of the anti-chikungunya potential of *Psidium guajava* leaf extract and their synthesized silver nanoparticles. *Virus Dis.* **2021**, *32*, 260–265. [CrossRef]
28. Imran, M. Optimization of ecofriendly synthesis of Ag nanoparticles by *Linum* usitatissimum hydrogel using response surface methodology and its biological applications. *Mater. Today Commun.* **2021**, *29*, 102789. [CrossRef]
29. Ali, F.; Ali, Z.; Younas, U.; Ahmad, A.; Mooin-Ud-Din, G.; Pervaiz, M.; Luque, R.; Ahmad, I.; Ashraf, A.; Albaqami, M.D.; et al. UV-Light Mediated Biosynthesis of Silver Nanowires; Characterization, Dye Degradation Potential and Kinetic Studies. *Sustainability* **2021**, *13*, 13220. [CrossRef]
30. Abdel-Aziz, H.M.; Farag, R.S.; Abdel-Gawad, S.A. Carbamazepine removal from aqueous solution by green synthesis zero-valent iron/Cu nanoparticles with *Ficus Benjamina* leaves' extract. *Int. J. Environ. Res.* **2019**, *13*, 843–852. [CrossRef]
31. Imran, M.; Saeed, Z.; Pervaiz, M.; Mehmood, K.; Ejaz, R.; Younas, U.; Nadeem, H.A.; Hussain, S. Enhanced visible light photocatalytic activity of TiO_2 co-doped with Fe, Co, and S for degradation of Cango red. *Spectrochim. Acta Part A Mol. Biomol. Spectrosc.* **2021**, *255*, 119644. [CrossRef]
32. Alshehri, A. Biofabrication of Fe nanoparticles in aqueous extract of *Hibiscus sabdariffa* with enhanced photocatalytic activities. *RSC Adv.* **2017**, *7*, 25149–25159. [CrossRef]
33. Pan, Z.; Lin, Y.; Sarkar, B.; Owens, G.; Chen, Z. Green synthesis of iron nanoparticles using red peanut skin extract: Synthesis mechanism, characterization and effect of conditions on chromium removal. *J. Colloid Interface Sci.* **2020**, *558*, 106–114. [CrossRef]
34. Jayandran, M.; Haneefa, M.M.; Balasubramanian, V. Green synthesis and characterization of *Manganese* nano-particles using natural plant extracts and its evaluation of antimicrobial activity. *J. Appl. Pharm. Sci.* **2015**, *5*, 105–110. [CrossRef]
35. Chouhan, S.; Guleria, S. Green synthesis of AgNPs using Cannabis sativa leaf extract: Characterization, antibacterial, anti-yeast and α-amylase inhibitory activity. *Mater. Sci. Energy Technol.* **2020**, *3*, 536–544. [CrossRef]
36. Jain, R.; Mendiratta, S.; Kumar, L.; Srivastava, A. Green synthesis of iron nanoparticles using *Artocarpus heterophyllus* peel extract and their application as a heterogeneous Fenton-like catalyst for the degradation of *Fuchsin* Basic dye. *Curr. Res. Green Sustain. Chem.* **2021**, *4*, 100086. [CrossRef]
37. Hoseinpour, V.; Souri, M.; Ghaemi, N. Green synthesis, characterisation, and photocatalytic activity of manganese dioxide nanoparticles. *Micro Nano Lett.* **2018**, *13*, 1560–1563. [CrossRef]
38. Shaker, K.; AbdAlsalm, A. Synthesis and Characterization Nano Structure of MnO_2 via Chemical Method. *Eng. Technol. J.* **2018**, *36*, 946–950. [CrossRef]
39. Chopra, N.; Claypoole, L.; Bachas, L.G. Morphological control of Ni/NiO core/shell nanoparticles and production of hollow NiO nanostructures. *J. Nanopart. Res.* **2010**, *12*, 2883–2893. [CrossRef]
40. Ljubas, D.; Smoljanić, G.; Juretić, H. Degradation of *Methyl Orange* and *Congo Red* dyes by using TiO_2 nanoparticles activated by the solar and the solar-like radiation. *J. Environ. Manag.* **2015**, *161*, 83–91. [CrossRef]

41. Cyril, N.; George, J.B.; Joseph, L.; Sylas, V.P. Catalytic Degradation of *Methyl Orange* and Selective Sensing of Mercury Ion in Aqueous Solutions Using Green Synthesized Silver Nanoparticles from the Seeds of *Derris trifoliata*. *J. Clust. Sci.* **2019**, *30*, 459–468. [CrossRef]
42. Shahwan, T. Green synthesis of iron nanoparticles and their application as a Fenton-like catalyst for the degradation of aqueous cationic and anionic dyes. *Chem. Eng. J.* **2011**, *172*, 258–266. [CrossRef]
43. Singh, H.P.; Gupta, N.; Sharma, S.K.; Sharma, R.K. Synthesis of bimetallic Pt–Cu nanoparticles and their application in the reduction of rhodamine B. *Colloids Surfaces A Physicochem. Eng. Asp.* **2013**, *416*, 43–50. [CrossRef]
44. Jegadeesan, G.B.; Amirthavarshini, S.; Divya, J.; Gunarani, G. Catalytic peroxygen activation by biosynthesized iron nanoparticles for enhanced degradation of Congo red dye. *Adv. Powder Technol.* **2019**, *30*, 2890–2899. [CrossRef]
45. Kamran, U.; Bhatti, H.N.; Iqbal, M.; Jamil, S.; Zahid, M. Biogenic synthesis, characterization and investigation of photocatalytic and antimicrobial activity of manganese nanoparticles synthesized from *Cinnamomum* verum bark extract. *J. Mol. Struct.* **2018**, *1179*, 532–539. [CrossRef]